THE EFFECT OF IRON BINDING ON THE CONFORMATION OF TRANSFERRIN

A Small Angle X-Ray Scattering Study

F. KILÁR AND I. SIMON
Institute of Enzymology, Biological Research Center, Hungarian Academy of Sciences, Budapest H-1502 Hungary

ABSTRACT Distance distribution functions, $p(r)$, radii of gyration, R_g, and radii of gyration of cross section, R_q, of apotransferrin, monoferric transferrin, and diferric transferrin have been compared. The alteration of R_g and R_q upon iron binding has been determined by a difference method. An unusual feature of the stepwise structural changes of transferrin upon iron saturation is that binding of the first ferric ion is responsible for more than half of the whole change in R_q, whereas R_g alters significantly only after the binding of the second ferric ion.

INTRODUCTION

Human serum transferrin is an iron transport glycoprotein (Mol wt = 80,000) that mediates iron exchange between tissues. Only preliminary crystallographic data are available for human plasma transferrin (1). The 0.6-nm–resolution electron density map of diferric rabbit plasma transferrin shows a well defined volume of high electron density with approximate maximum dimensions of 9.5 × 6 × 5 nm. The model constructed from this map shows that the molecule consists of two lobes, i.e. structural domains, of roughly equal size. The major axes of these lobes are inclined at ~30° to one another (2).

The transferrin molecule contains two iron binding sites. One is located in the *N*-terminal lobe, the other in the *C*-terminal one (3). The two binding sites have different affinities for iron; at neutral pH the one on the *C*-terminal lobe has significantly higher affinity to ferric ion than the other one (4).

Data about the conformation of transferrin in solution and for the conformational changes upon iron binding are rather scarce. A small-angle neutron scattering study indicates that apotransferrin has an oblate spheroidal shape with semi-axes of length 4.66 nm, 4.66 nm, and 1.58 nm and a radius of gyration R_g = 3.025 ± 0.049 nm (5). Early hydrodynamic measurements showed that transferrin became more compact after saturation with iron (6).

In this work the shape and size of apotransferrin and its stepwise conformational changes upon iron binding have been studied.

EXPERIMENTAL PROCEDURES

Materials

Transferrin, from pooled human sera, was obtained from Boehring-Werke AG (Marburg) and was used without further purification. The chelatin agent nitrilotriacetic acid (NTA) was a Fluka (Buchs) product. All other reagents were Reanal (Budapest) products of reagent grade.

Monoferric and diferric transferrin were prepared by addition of stoichiometric amounts of $Fe(NTA)_2^{3-}$ to apotransferrin, as described previously (7–9). All transferrin samples used in the small angle x-ray scattering experiments were in 10 mM Tris-HCl buffer, pH 7.4.

The homogeneity and purity of samples were checked by urea gel electrophoresis according to the method of Makey and Seal (10).

Small Angle X-Ray Scattering

Small angle x-ray scattering experiments were carried out with a Dron-1 type x-ray analytical instrument (USSR) combined with a Shimadzu small angle camera (Japan). Cu K_α x-ray (λ = 0.154 nm) was used, the Cu K_β line was removed by Ni filter and the continuous part of the spectrum was eliminated by a difference discriminator. Collimation correction, based on Lake's iteration procedure, was made as reported recently (11).

Distance distribution function, $p(r)$, was calculated from the corrected $I(2\theta)$ function. Maximum dimension of the macromolecule, D_{max}, where the $p(r)$ function reaches the zero value was determined from $p(r)$ (12). The radii of gyration and radii of gyration of cross section were also determined from the slope of the Guinier plots (13), i.e. log I vs. $(2\theta)^2$, in the range of 5–13 mrad, and log $[I \times (2\theta)]$ vs. $(2\theta)^2$ respectively, in the range of 15–21 mrad.

The change in the radii of gyration upon iron binding was monitored by a sensitive difference method (14). The essence of this method is that the plot log I_a/I_b vs. $(2\theta)^2$ gives a straight line at small angles ($2\theta \rightarrow 0$) the slope of which is proportional to ΔR_g

$$\Delta R_g = R_{g,a} \frac{p_g}{2P_{g,a}},$$

where I_a and I_b are the scattering intensities obtained from state a and b of the macromolecule, respectively, $R_{g,a}$ is the radius of gyration of the

Dr. Kilár's present address is Department of Neurology and Psychiatry, University of Pécs Medical School, Pécs, Rét utca 2, H-7623 Hungary

macromolecule in state a, p_g is the slope of the difference plot and $P_{g,a}$ is the slope of the Guinier plot of the directly measured scattering curve in state a. The advantage of this difference plot in elimination of systematic errors due to finite slit dimensions, inhomogeneities of the incident beam along the entrance slit, and interparticular scattering has been discussed and demonstrated elsewhere (14–19).

Extension of Difference Method

The Guinier plot and difference plot give straight lines since the scattering curve, I, can be approximated by a gaussian function at small angles for any kind of scattering particles and the ratio of two gaussian functions is also a gaussian function. On the other hand, for particles with cylindrical symmetry in a certain range of 2θ, $[I \times (2\theta)]$ becomes a gaussian-like function i.e. log $[I \times (2\theta)]$ vs. $(2\theta)^2$ is a straight line, the slope of which is proportional to R_q. Replacing I by $[I \times (2\theta)]$ in the derivation of ref. 14, it is evident that for these particles, in the range of 2θ where log $[I \times (2\theta)]$ vs. $(2\theta)^2$ gives a straight line, i.e. where $[I \times (2\theta)]$ is a gaussian-like function, log I_a/I_b vs. $(2\theta)^2$ is a straight line, the slope of which is proportional to the change of R_q

$$\Delta R_q = R_{q,a} \frac{p_q}{2P_{q,a}},$$

where $R_{q,a}$ is the R_q of the particle in state a, p_q is the slope of the difference plot (in the range where log $[I \times (2\theta)]$ vs. $(2\theta)^2$ results in a straight line) and $P_{q,a}$ is the slope of plot log $[I \times (2\theta)]$ vs. $(2\theta)^2$.

It is worth noting that the small change in the thickness factor R_d of lamellar particles can also be determined from the slope of the difference plot, p_d, (in the range of 2θ where the log $[I \times (2\theta)^2]$ vs. $(2\theta)^2$ plot is linear)

$$\Delta R_d = R_{d,a} \frac{p_d}{2P_{d,a}}.$$

RESULTS

The distance distribution functions, $p(r)$ – s, and the Guinier plots for various transferrin samples are shown in Figs. 1 and 2. Fig. 1 also shows two calculated $p(r)$ functions:

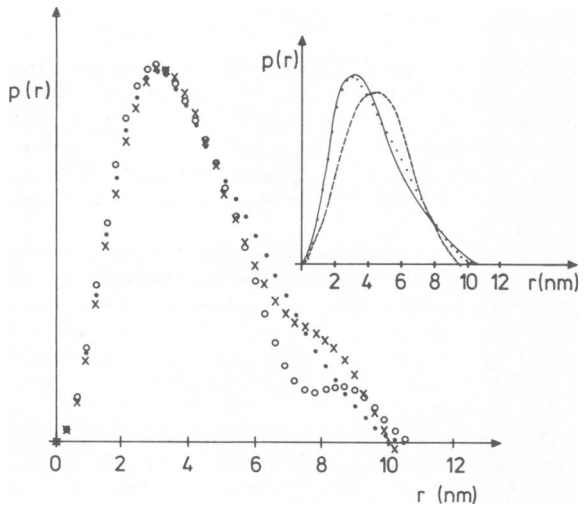

FIGURE 1 Distance distribution function, $p(r)$, of apotransferrin (●●●), monoferric transferrin (xxx), and diferric transferrin (OOO). Insert: apotransferrin (●●●), solid line was calculated for a circular cylinder of diameter 4.8 nm, length 9.6 nm; and dashed line was calculated for an oblate spheroid with semi-axes of length 4.66 nm, 4.66 nm, and 1.58 nm, as proposed by Martel et al. (5).

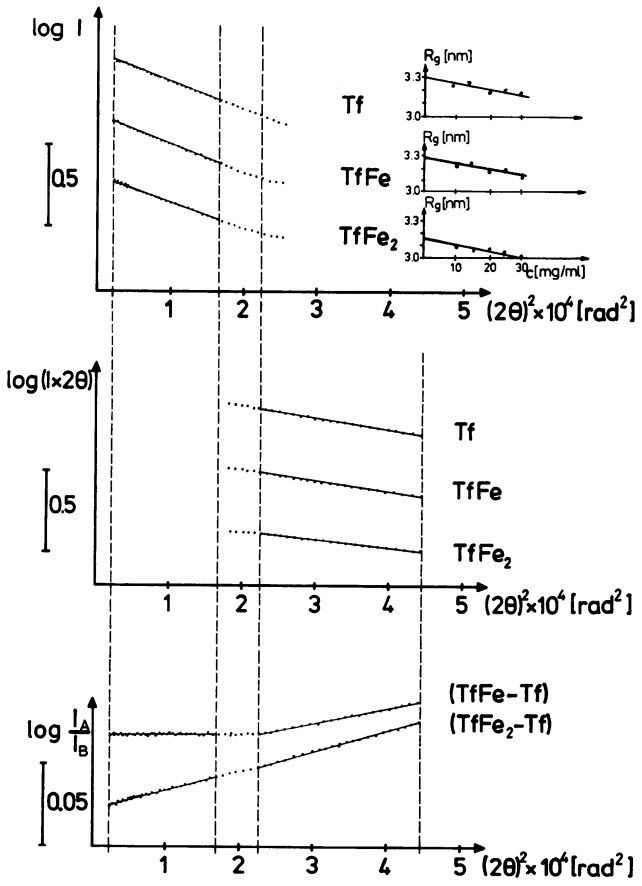

FIGURE 2 Guinier plots for determination of R_g and R_q of various transferrin samples: log I vs. $(2\theta)^2$ and log $(I \times 2\theta)$ vs. $(2\theta)^2$; and difference plots for determination of changes of R_g and R_q upon iron saturation: log (I_A/I_B) vs. $(2\theta)^2$. Vertical dashed lines indicate domains from where R_g, R_q, ΔR_g, and ΔR_q values are obtained. Protein concentration is 25 mg/ml. Insert: concentration dependence of the apparent radii of gyration, R_g.

that of a circular cylinder with diameter 4.8 nm and length 9.6 nm, and that of the model suggested by Martel et al. (5). The apparent D_{max}, R_g, and R_q values have been determined in the range of 10–30 mg/ml protein concentration and extrapolated to zero concentration. Concentration dependence of the apparent radii of gyration, R_g, is shown in the insert of Fig. 2. No significant concentration dependence of D_{max} and R_q was observed. The extrapolated values of D_{max}, R_g, and R_q are listed in Table I.

TABLE I
DATA FOR APOTRANSFERRIN AND ITS IRON COMPLEXES

Protein	Maximum dimensions (D_{max})	Radii of gyration (R_g)	Radii of gyration of cross section (R_q)
	nm	*nm*	*nm*
Apotransferrin	10.5 ± 0.5	3.30 ± 0.03	1.71 ± 0.04
Monoferric transferrin	10.4 ± 0.5	3.28 ± 0.03	1.62 ± 0.04
Diferric transferrin	10.7 ± 0.5	3.15 ± 0.03	1.60 ± 0.04

By the aid of the sensitive difference method a more detailed picture on the alteration of R_g and R_q upon iron binding has been obtained. (Fig. 2.) The formation of monoferric transferrin results in no measurable changes in R_g, ΔR_g is <0.007 nm, while R_q is decreased by a value of $\Delta R_q = 0.09 \pm 0.01$ nm. Upon binding of two ferric ions to apotransferrin the R_g and R_q values decreased by $\Delta R_g = 0.11 \pm 0.007$ nm and $\Delta R_q = 0.13 \pm 0.01$ nm, respectively.

DISCUSSION

The radius of gyration of apotransferrin was found to be similar to that published earlier in a small angle neutron scattering study (5). The difference, which is <10%, may be a consequence of the different conditions and techniques used.

The $p(r)$ function shows that if there is any simple geometric form that approximates the apotransferrin molecule, it is a prolate cylinder the length of which is twice as large as its diameter, rather than an oblate ellipsoid of revolution (1:1:0.34) suggested by Martel et al. (5). (Fig. 1.) For a cylinder with a diameter of 4.8 nm and length of 9.6 nm R_g, R_q, and D_{max} are 3.3 nm, 1.7 nm, and 10.7 nm respectively (see Table I), which agrees with the maximum dimensions of the volume of high electron density found by crystallographers (2). On the other hand, both the model constructed from the preliminary crystallographic data (2) and the deviation of the observed $p(r)$ function from that calculated for the best-fitting cylinder show that the shape of apotransferrin is more complicated than a simple cylinder.

Our data indicating that transferrin becomes more compact upon iron saturation are in good agreement with the early hydrodynamic data (6).

The stepwise structural changes of transferrin upon iron binding exhibit an apparently unusual feature. Binding of the first ferric ion to the *C*-terminal lobe is responsible for more than half of the total change in R_q, while R_g alters significantly only after the binding of the second ferric ion.

This phenomenon can not be explained unambiguously from the data available. One of the possible explanations consistent with our data is the following: The decrease of R_g and R_q upon iron saturation indicates that binding of ferric ion(s) results in a more compact protein molecule. Binding of the first ferric ion to the apotransferrin may be responsible for a significant part of the conformational change corresponding to the iron saturation process. On the other hand, binding of one ferric ion to the apotransferrin molecule consisting of two similar lobes may induce asymmetry in the protein molecule. Bringing in asymmetry, as a rule, results in an increase of the R_g of a particle. The latter effect may compensate the decrease of R_g upon binding of the first ferric ion and significant reduction of R_g value can be observed when the transferrin molecule becomes symmetrical again after binding of the second ferric ion.

Considering the changes in the $p(r)$ function upon iron saturation, one can speculate on the nature of the conformational changes. The changes of $p(r)$ are mainly localized in the second half of the $p(r)$ function ($r > 1/2\ D_{max}$). This may indicate that iron binding alters the relative position of the two lobes of the transferrin molecule rather than the structure of the lobes. Iron saturation hardly alters the value of D_{max}, i.e. the distance of the lobes may not change appreciably; iron binding may rather result in some kind of twisting of the two lobes relative to each other.

We are grateful to Dr. P. Závodszky for his support and interest during this work. The helpful discussion with Dr. L. Cser and Dr. F. Vonderviszt are acknowledged in gratitude. Thanks are due to Prof. L. A. Feigin for his comments during the preparation of the manuscript. We are indebted to Ms. J. Balczer and Ms. Z. Török for their skillful technical assistance.

Received for publication 3 January 1985 and in final form 26 June 1985.

REFERENCES

1. DeLucas, L. J., F. L. Suddath, R. A. Gams, and C. E. Bugg. 1978. Preliminary x-ray study of crystals of human transferrin. *J. Mol. Biol.* 123:285–286.
2. Gorinsky, B., C. Horsburg, P. F. Lindley, D. S. Moss, M. Parkar, and J. L. Watson. 1979. Evidence for the bilobal nature of differic rabbit plasma transferrin. *Nature (Lond.).* 281:157–158.
3. Brock, J. H., F. Arzabe, F. Lampreave, and A. Pineiro. 1976. The effect of trypsin on bovine transferrin and lactoferrin. *Biochim. Biophys. Acta.* 446:214–225.
4. Yeh, S. M., and C. F. Meares. 1980. Characterization of transferrin metal-binding sites by diffusion-enhanced energy transfer. *Biochemistry.* 19:5057–5062.
5. Martel, P., S. M. Kim, and B. M. Pawell. 1980. Physical characteristics of human transferrin from small-angle neutron scattering. *Biophys. J.* 31:371–380.
6. Rossenau-Motreff, M. Y., F. Soetewey, R. Lamote, and H. Peeters. 1971. Size and shape determination of apotransferrin and transferrin monomers. *Biopolymers.* 10:1039–1048.
7. Evans, R. W., and J. Williams. 1978. Studies of the binding of different iron donors to human serum transferrin and isolation of iron-binding fragments from the N and C Terminal Regions of the protein. *Biochem. J.* 173:543–552.
8. Bates, G. W., and M. R. Schlaback. 1973. The reaction of ferric salt with transferrin. *J. Biol. Chem.* 248:3228–3232.
9. Aisen, P., A. Leibman, and J. Zweier. 1978. Stoichometric and site characteristics of the binding of iron to human transferrin. *J. Biol. Chem.* 253:1930–1937.
10. Makey, D. G., and U. S. Seal. 1976. The detection of four molecular forms of human transferrin during the iron binding process. *Biochim. Biophys. Acta.* 453:250–256.
11. Kilár, F., I. Simon, S. Lakatos, F. Vonderviszt, G. A. Medgyesi, and P. Závodszky. 1985. Solution conformation of the four human IgG subclasses: small angle x-ray scattering and hydrodynamic studies. *Eur. J. Biochem.* 147:17–25.
12. Glatter, O., and O. Kratky. 1982. Small Angle X-ray Scattering. Academic Press, Inc., London. 167.
13. Guinier, A., and G. Fournet. 1955. Small Angle Scattering of X-Rays. John Wiley & Sons, Inc., New York. 127.
14. Simon, I. 1971. Determination of small alterations in the radius of gyration by small-angle x-ray scattering *J. Appl. Cryst.* 4:317–318.

15. Simon, I. 1972. Study of the position of NAD and its effect on the conformation of d-glyceraldehyde-3-phosphate dehydrogenase by small-angle x-ray scattering. *Eur. J. Biochem.* 30:184–189.
16. Simon, I., S. Mora, and P. Elödi. 1974. Studies on the active centre of pancreatic amylase. II. Small angle x-ray scattering investigation. *Mol. Cell. Biochem.* 4:211–216.
17. Stamatoff, J. B. 1979. An approach for time-resolved x-ray scattering. *Biophys. J.* 26:325–328.
18. Borso, C. S., and J. B. Stamatoff. Modification of the apparent radius of gyration of cytochrome-c by the distribution of counterions in solution. *Biopolymers.* 19:1887–1897.
19. Pilz, I., O. Glatter, and O. Kratky. 1979. Small-angle x-ray scattering. *Methods Enzymol.* 61:148–249.